Nonwetting Behavior of Al–Co Quasicrystalline Approximants Owing to Their Unique Electronic Structures

Kanika Anand, Vincent Fournée, Geoffroy Prévot, Julian Ledieu, Emilie Gaudry

Non-Wetting Behavior of Al-Co Quasicrystalline Approximants Owing to their Unique Electronic Structures

Kanika Anand[1,2], Vincent Fournée[1], Geoffroy Prévot[3], Julian Ledieu[1], Émilie Gaudry[1*]

[1] *Université de Lorraine, CNRS, IJL, F-54000 Nancy, France*

[2] *CIRIMAT, Université de Toulouse, CNRS, INPT, UPS, 4 Allée Emile Monso, BP44362, 31030 Toulouse Cedex 4, France*

[3] *Sorbonne Université, CNRS, Institut des NanoSciences de Paris, 4 place Jussieu, 75005 Paris, France*

E-mail: emilie.gaudry@univ-lorraine.fr

Table of Contents Graphic

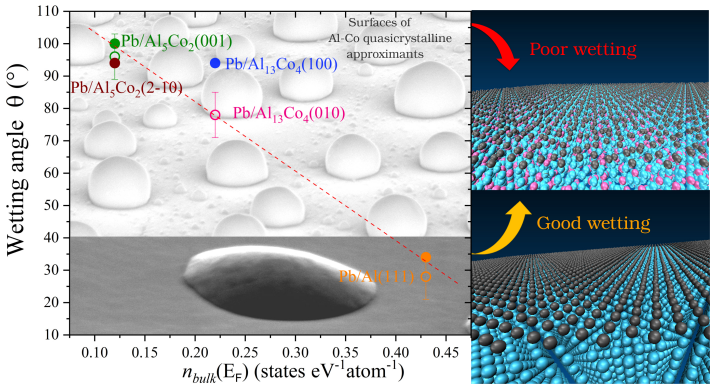

KEYWORDS: Wetting, Contact Angle, Interfacial Energy, Quasicrystalline Approximant Surfaces, Electronic Structures, Scanning Electron Microscopy, Density Functional Theory

Abstract

Good wetting is generally observed for liquid metals on metallic substrates, while poor wetting usually occurs for metals on insulating oxides. In this work, we report unexpected large contact angles for lead on two metallic approximants to decagonal quasicrystals, namely Al_5Co_2 and $Al_{13}Co_4$. Intrinsic surface wettability is predicted from first-principles, using a thermodynamic model based on the Young equation, and validated by the good agreement with experimental measurements performed under ultra-high vacuum by scanning electron microscopy. The atomistic details of the atomic and electronic structures at the Pb-substrate interface, and the comparison with Pb(111)/Al(111), underlines the influence of the specific electronic structures of quasicrystalline approximants on wetting. Our work suggests a possible correlation of the contact angles with the density of states at the Fermi energy and paves the way for a better fundamental understanding of wettability on intermetallic substrates, which has potential consequences in several applications, like supported catalysts, protective coatings or crystal growth.

1 Introduction

The design of metallic alloys with specific wetting properties is crucial for numerous technological applications. Efficient hydrophobic attributes are required for anti-icing surfaces,[1–4] self-cleaning materials[5–7] or corrosion-resistant layers.[4,8,9] The way a liquid wets a solid is also decisive for crystal growths,[10,11] solidification processes[12,13] or joining technologies.[14] For some applications, the targeted wetting characteristics can be reached artificially by the preparation of surfaces with complex textures and architectures,[15,16] or by the deposition of molecular layers with specific properties.[17,18] Much less efforts have focused on the development of metallic alloys with specific intrinsic wetting properties.

Wetting properties are quantified through contact angles, i.e. angles where a liquid-vapor interface meets a solid surface. For non-reactive metal liquids on solids, the intrinsic contact angles results from two types of competing forces: adhesion forces between the liquid and the solid phases and cohesion forces of the liquid.[19] Then, in the absence of barriers to wetting such as oxide films, good wetting, i.e. contact angles of a few degrees or tens of degrees, is observed if the interactions occurring at the interface are significant. This is fulfilled for liquid metals on metallic substrates because in this type of systems the interfacial bond is strong (metallic).[20]

Unexpected large contact angles have been measured for several liquids deposited on Al-based quasicrystalline alloys, i.e. intermetallic compounds characterized by long-range atomic order with no periodicity.[21,22] In these experiments, the substrates were however covered by a very thin surface layer of alumina oxide, which avoided the determination of their intrinsic wetting properties. The outstanding values of the contact angles were then attributed to a combination of intrinsic and extrinsic factors, namely the specific electronic density of states within the bulk material, underneath the oxide layer, and the thickness of the oxide layer.

A few attempts have been carried out to disentangle the intrinsic contributions of the Al-based quasicrystalline substrate from those of the oxide layer.[23,24] From the experimental

point of view, such goal is challenging. It requires ultra-high vacuum (UHV) conditions and a careful preparation of the system : deposition of a metal thin film on a clean surface free from any contaminants, *in situ* de-wetting leading to the formation of droplets and determination of the contact angle using Scanning Electron Microscopy (SEM). On the other hand, intrinsic wetting properties of quasicrystalline surfaces can be determined through theoretical calculations, based on the droplet method or on free energy calculations. Such approaches have been widely used to determine contact angles and interfacial energies of a large variety of systems.[25–27] However, in most cases, the simulations largely rely on classical potentials. This may lead to interfacial energies (γ) and contact angles (θ) significantly different from the ones determined experimentally, even for simple systems such as Pb(111)/Al(111) – $\gamma^{calc}_{\mathrm{Pb/Al(111)}}$ = 28.3 meV/Å^2 ($\gamma^{exp}_{\mathrm{Pb(111)/Al(111)}}$ = 13.5 ± 2 meV/Å^2),[28,29] $\theta^{calc}_{\mathrm{Pb/Al}}$=46.4^o ($\theta^{exp}_{\mathrm{Pb/Al(111)}}$=27.3 ± 0.8^o)[28,30] – which questions the possibility of assessing accurate values of contact angles from classical potentials which do not explicitly consider electronic effects.

In this work, using liquid lead as a probe, we identify notable intrinsic low wetting behaviors, i.e. contact angles close to or larger than 90^o, for two intermetallic substrates considered as approximants to decagonal quasicrystals, namely Al_5Co_2 and $Al_{13}Co_4$. A quantitative and predictive method to evaluate the intrinsic contact angles, applicable to a broad range of intermetallic substrates and validated by the good agreement with a few experimental measurements, is proposed, based on the Young equation combined with Density Functional Theory (DFT). Electronic effects are found to have a significant influence on the wetting properties of the considered quasicrystalline-related substrates. Our study suggests a possible correlation of the contact angles with the density of states at the Fermi energy. It opens a way to design intermetallic alloys with targeted wetting properties based on this factor.

2 Methods and Materials

2.1 Experimental Details

The two approximant substrates used in this study were extracted from single crystals grown by the Czochralski technique, as detailed in Ref.[31] for Al_5Co_2 and in Ref.[32] for $Al_{13}Co_4$. The $Al_{13}Co_4(010)$ and $Al_5Co_2(001)$ surfaces were prepared under UHV (base pressure of 2×10^{-10} mbar) by repeated cycles of Ar^+ sputtering and annealing, as described in Refs.[31,33] The structures of the clean surfaces were checked by low-energy electron diffraction prior to Pb deposition.

Lead was then dosed on the clean surfaces for a few minutes using a Knudsen cell, to form a thick uniform layer on the substrates. The pressure was kept in the low 10^{-9} mbar range, during the deposition. Samples were further heated slightly above the melting point of Pb (T=357 ^{o}C, T_m^{Pb}=327 ^{o}C) to produce liquid droplets of micrometer size or smaller. The temperature was then decreased gradually to room temperature.

Auger spectra in between the droplets indicate the presence of some O contamination, as well as the presence of a Pb wetting layer still covering the substrate after the formation of the droplets, in agreement with previous observations (Fig. S1).[28] Contact angles were further determined from in situ SEM imaging at room temperature, with a tilt angle between the surface normal and the in-lens secondary electron detector up to 70^o (NanoSEM/SAM, ScientaOmicron). High resolution micrographs were analyzed by means of standard ImageJ software, based on a circular-curve fitting (Tab. S1 and Fig. S2).

2.2 Computational Details

All calculations are based on DFT and use the Vienna *ab initio* simulation package (VASP). Self-consistent Kohn Sham equations were solved by means of the projected-augmented wave (PAW) method.[34,35] Atomic structures were relaxed using the conjugate gradient method until the forces are lower than 0.02 eV/Å. The considered systems were modeled with *p*-

layer thick slabs separated by a void thickness equal to 15 Å (p = 6 for $Al_5Co_2(2\bar{1}0)$, p = 7 for $Al_5Co_2(001)$ and $Al_{13}Co_4(100)$ and p = 9 for Al(111)). The plane-waves energy cut-off was set to 450 eV. Monkhorst-Pack meshes were used for the k-points sampling:[36] 5×5×1 for Pb/Al(111) (Moiré structure), 1×7×7 for $Pb/Al_{13}Co_4(100)$, 7×7×1 for $Pb/Al_5Co_2(001)$ and 1×3×11 for $Pb/Al_5Co_2(2\bar{1}0)$. Finer k-point grids were used for density of states calculations. Our approach adopts the standard semilocal PBE functional.[37,38] Within this approximation, cell parameters, cohesive energies of bulk systems as well as surface energies of oriented crystals are in good agreement with the literature[39–41] (Tabs. S2 and S3).

2.3 Bulk and Clean Surface Structures

The Al_5Co_2 and $Al_{13}Co_4$ compounds crystallize in the $P6_3/mmc$ (No. 194, hP28)[42] and $Pmn2_1$ (No. 31, oP102)[43] space groups, respectively. Both structures can be described by a stacking of two types of layers (either flat or corrugated layer), that alternate perpendicular to [100] for $Al_{13}Co_4$, and perpendicular to [2-10] and [001] for Al_5Co_2 (Fig. S3).

The clean surface structures have been deduced from a combination of surface science studies under UHV and theoretical calculations.[31,33,44–46] The two considered low index surface structures of Al_5Co_2 arise from a surface termination at incomplete puckered layers with specific atomic arrangements missing, thus forming reconstructions (Fig. 1). The $Al_{13}Co_4(100)$ surface structure results from a plane selection and consists of dense Al-rich layers with surface Co atom missing (Fig. 1).[33,45,46] In all cases, the termination layer is Al-rich, and the average terrace size is of the order of 0.1 μm as observed by STM.

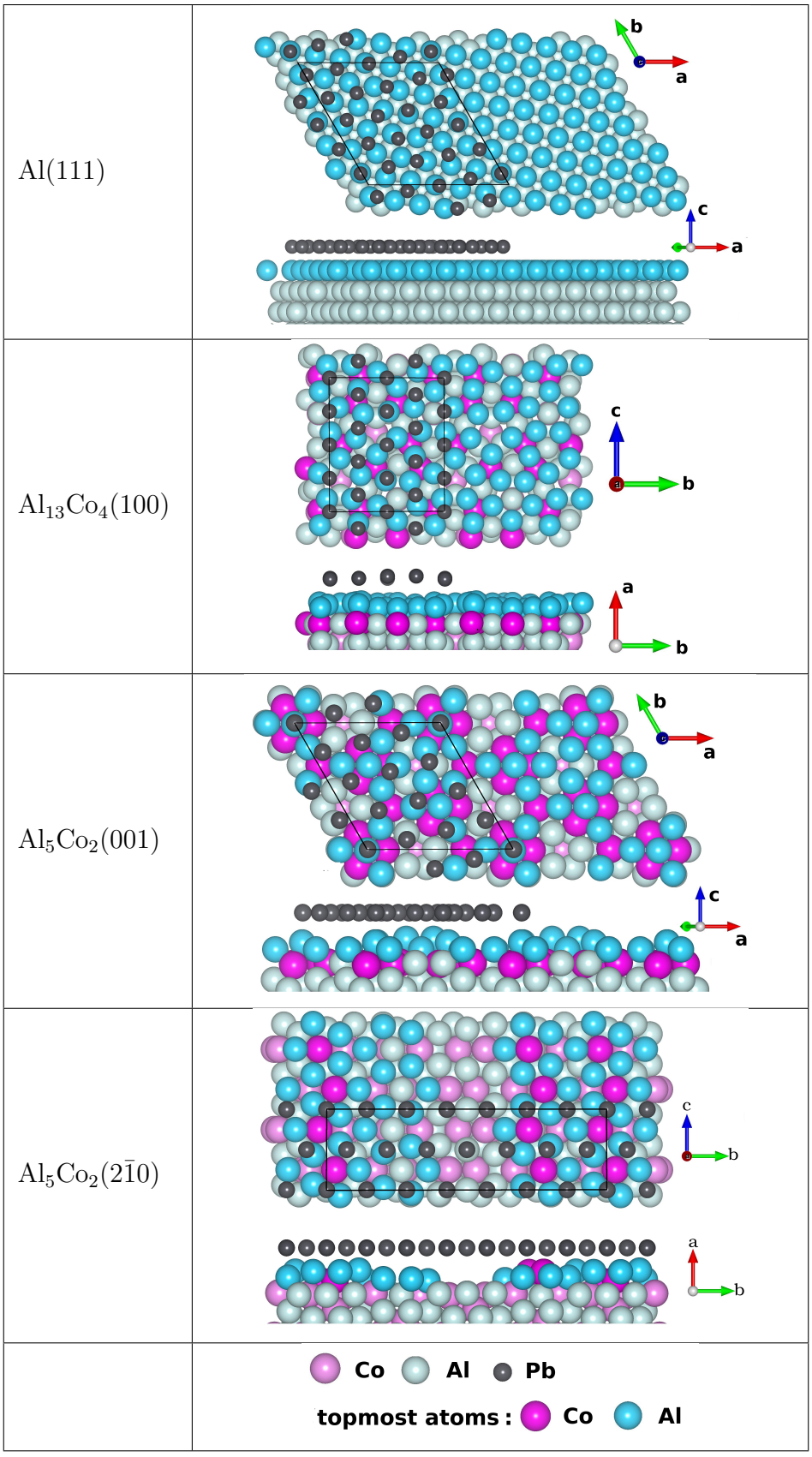

Figure 1: Structures of the Al(111), $Al_{13}Co_4(100)$ $Al_5Co_2(001)$ and $Al_5Co_2(2\bar{1}0)$ surfaces, along with the corresponding lead interfaces (before structural relaxation).

2.4 Interfaces: Thermodynamic Approach and Structural Models

Two types of simulations methods are generally used to determine contact angles.[47] Similarly to the experimental approach, the droplet method consists in considering a liquid droplet on a surface. When a well-defined shape is obtained by simulations, the contact angle is calculated. The previous method may however suffer from finite size effects (line tension, interfacial curvature, or arbitrary choice of the solid-fluid contact plane). Methods based on free energy calculations are not as straightforward as the droplet simulations, but tend to provide more accurate contact angle estimates.[48]

Here, the contact angles are determined through the Young equation (Fig. 2),[49,50] which involves surface ($\gamma^{\text{substrate}}$) and interfacial ($\gamma^{\text{interface}}$) energies:

$$\cos\theta = \frac{\gamma^{\text{substrate}} - \gamma^{\text{interface}}}{\gamma^{\text{Pb}}} \tag{1}$$

The surface energy of lead in the previous equation is taken to be the one of Pb(111) ($\gamma_{\text{Pb}} = \gamma_{\text{Pb(111)}}$). This assumption is supported by the temperature at which the experimental measurements were performed (Pb is solid at room temperature) and by the similar surface energies and electronic structures of dense liquid and fcc Pb.[51–53]

According to the scheme shown in Fig. 2, the interfacial energy is given by

$$\gamma^{\text{interface}} = \frac{E^{tot}_{system} - A \times (\gamma^{\text{Pb(111)}} + \gamma^{\text{substrate}}) - \sum_{\mathcal{X}} n_{\mathcal{X}} \times \mu^{\mathcal{X}}}{A} \tag{2}$$

where E^{tot}_{system}, $\mu^{\mathcal{X}}$, $\gamma^{\text{substrate}}$, $\gamma^{\text{Pb(111)}}$, $n_{\mathcal{X}}$ and A are the total energy of the considered system, the chemical potentials of the $\mathcal{X}$ species ($\mathcal{X}$ = Pb, Co, Al), the surface energy of the substrate (Tabs. S2, S3 and 2), the surface energy of Pb(111) (17.8 meV/Å^2), the number of $\mathcal{X}$ atoms in the system and the interfacial area, respectively. Since the intermetallic compounds are synthesized from an Al-rich melt, the Al chemical potential is taken as the one of bulk Al in the previous equations ($\gamma^{\text{substrate}}$, $\mu^{\mathcal{X}}$).

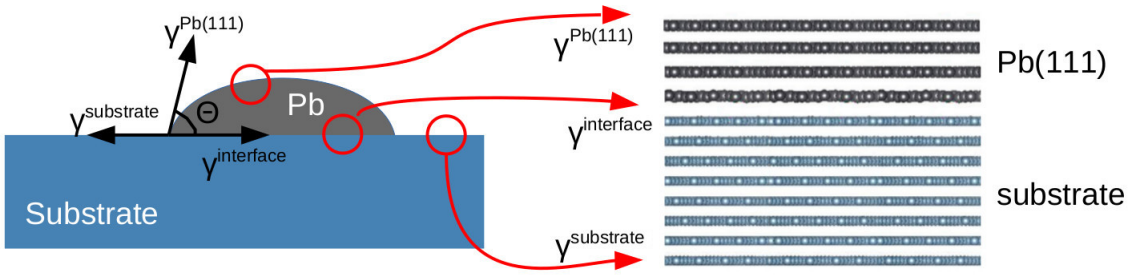

Figure 2: Schematic diagram to predict the surface wettability of Al-based approximants by lead. The surface energies of the substrate and lead are calculated separately, and used in equations 1 and 2 to evaluate the interfacial energy (DFT slab model, right-hand side).

Experimentally, lead is observed in between the Pb droplets. The surface energy of the substrate has then to be corrected from Pb adsorption, as already shown by Ref.:[28]

$$\gamma^{\text{substrate}}_{modified} = \gamma^{\text{substrate}} + \frac{E_{ads}}{A} \quad \text{with} \quad E_{ads} = E^{tot}_{slab+1\,Pb\text{-}layer} - E^{tot}_{substrate} - n_{\text{Pb}} \times E^{\text{Pb}}_{coh} \qquad (3)$$

where $E^{tot}_{slab+1\,Pb\text{-}layer}$, $E^{tot}_{substrate}$ and E^{Pb}_{coh} are the total energies of the substrate covered with an Pb atomic layer, the total energy of the clean substrate and the lead cohesive energy ($E^{\text{Pb}}_{coh} = \mu^{\text{Pb}}$).

The previous approach is based on slab models, built with a substrate covered by n-layer thick dense Pb(111) films (hexagonal-like models), with $1 \leq n \leq 4$. For Pb(111)/Al(111), we considered a $(\sqrt{31} \times \sqrt{31})$R8.95^o higher-order commensurate structure relative to Al(111), corresponding to a $(\sqrt{21}\times\sqrt{21})$R10.9^o reconstruction of Pb(111) (lattice parameter 15.9 Å), in agreement with the experimental observations[54] (Fig. 1) as illustrated by the comparison of the simulated and experimental STM images (Fig. S4). The other interfaces have been built in order to minimize the lattice mismatch between Pb(111) and the considered substrate. It leads to a $(\sqrt{13} \times \sqrt{13})R13.9^o$ reconstruction of Pb(111) for Pb/Al_5Co_2(001), a $\begin{pmatrix} 7 & 1 \\ 0 & 2 \end{pmatrix}$ superstructure of Pb(111) for Pb/$Al_5Co_2(2\bar{1}0)$ and a $\begin{pmatrix} 4 & 0 \\ 2 & 4 \end{pmatrix}$ superstructure of Pb(111) for Pb/$Al_{13}Co_4$(100) (5%, 7% and 2.5% averaged lattice mismatches, respectively).

For $Pb/Al_{13}Co_4(100)$, in addition to the previous hexagonal-like Pb-adlayer models, we considered a 1-layer thick Pb-adlayer slab built by progressively filling all favorable adsorption sites.[55] The corresponding modified surface energy ($\gamma^{\text{substrate}}_{modified}$) calculated as a function of the Pb coverage, presents a discontinuity for a coverage equal to 0.090 at./Å^2 (Fig. 3): the modified surface energy increases abruptly, becoming larger that the one of a lead bilayer (15+1 at./surf. cell). This supports an optimal coverage equal to 15 atoms per cell for a single Pb-adlayer, in good agreement with the Pb coverage observed experimentally (0.090 at./Å^2).[56] This structural model was used to build a 4-layer thick Pb-adlayer slab, where the two first adlayers are pseudomorphic (15 Pb atoms/ surface cell) and the other two Pb-adlayers are dense (16 Pb atoms/ surface cell). We will refer to this model as the pseudomorphic-like Pb-adlayer model.

Finally, for $Pb/Al_{13}Co_4(100)$, models have also been built using interfacial structures derived from *ab initio* molecular dynamic (AIMD) simulations carried out in the canonical ensemble (total simulation time of runs = 50 ps, timestep = 1 fs, T=T_m^{Pb}=600 K), followed by a DFT-based conjugate-gradient structure optimization. We took simulation cells containing a 7-layer thick $Al_{13}Co_4(100)$ slab topped with a 6Å thick region filled with lead. The resulting structure was used to built 4-layer thick Pb-adlayers slabs (the first two Pb-adlayers come from AIMD and the other two Pb-adlayers are dense layers). We will refer to this model as the MD-like Pb-adlayer model.

3 Results

3.1 Contact Angles

Contact angles are experimentally measured for Pb/Al(111), $Pb/Al_{13}Co_4(010)$ and $Pb/Al_5Co_2(001)$ (Tab. 1 and Fig. 4), avoiding points very close to any crystal facet, as it would lead to misleading contact angles. The shape of the Pb droplets are typically spherical, after liquid de-wetting, with eventually small flat facets in narrow regions, attributed to the small

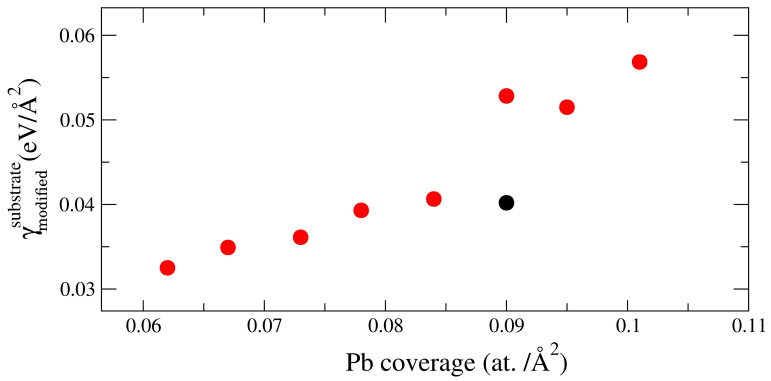

Figure 3: Modified surface energy of $Al_{13}Co_4(100)$, considering Pb atoms adsorbed at the surface, in the favorable adsorption sites identified in Refs[56,57] (single Pb layer, in red). The black points corresponds to a "bilayer" structure (15 + 1 Pb atoms / surf. cell).

anisotropy of the Pb surface energy. A non-wetting behavior is observed for $Pb/Al_5Co_2(001)$ and $Pb/Al_{13}Co_4(010)$, with contact angles of 96 ± 7 degrees and 78 ± 7 degrees, respectively, demonstrating the specific intrinsic wetting properties of the quasicrystalline approximant.

Table 1: Experimental (θ^{exp}) and theoretical (θ^{calc}) contact angles for Pb droplets on different substrates (hexagonal-like structures), along with the density of states ($n_{bulk}(E_F)$) at the Fermi energy, resulting from DFT calculations. [a] is the value for the P_{B-4Co} model (see Tab. S3). [b] and [c] are the values for the pseudomorphic-like and the MD-like structures, respectively (see text).

Substrate	θ^{exp} (^{o})	θ^{calc} (^{o})	$n_{bulk}(E_F)$ (states/(eV.atom))
Al(111)	28 ± 7	35	0.43
$Al_5Co_2(001)$	96 ± 7	100	0.12[31]
$Al_5Co_2(2\bar{1}0)$		94 (68[a])	0.12[31]
$Al_{13}Co_4(010)$	78 ± 7	-	0.22
$Al_{13}Co_4(100)$	-	94 (82[b], 116[c])	0.22

According to our thermodynamic model, the contact angles calculated for Pb/Al(111), $Pb/Al_5Co_2(001)$, $Pb/Al_5Co_2(2\bar{1}0)$ and $Pb/Al_{13}Co_4(100)$ are 35^o, 100^o, 94^o and 94^o, respectively, using hexagonal-like 4 layers models (Tab. 1). These values match our experimental observations when available, assessing the validity of our theoretical approach. For $Pb(111)/Al_{13}Co_4(100)$, our theoretical value is rather different from the value published

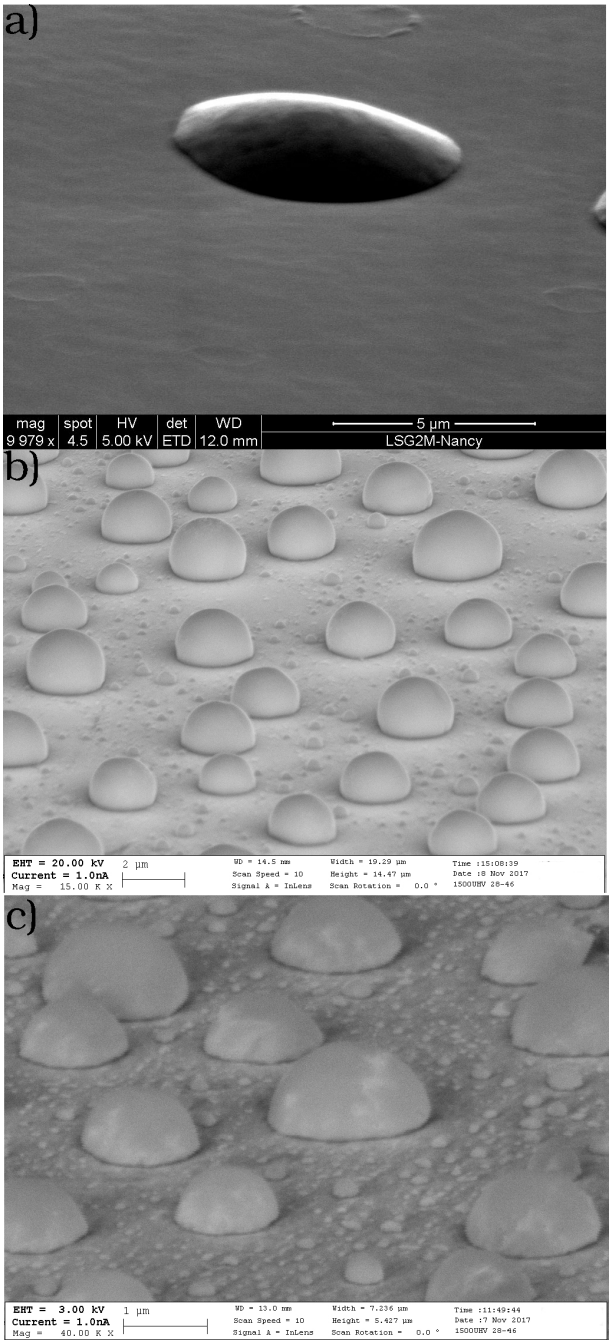

Figure 4: SEM micrographs showing Pb droplets on (a) Al(111), (b) Al_5Co_2(001) and (c) $Al_{13}Co_4$(010).

in Ref.[24] (45^o). Such discrepancy is attributed to the differences between the experimental and theoretical substrates. The calculation considered the single crystalline $Al_{13}Co_4$(100) homogeneous surface, while the experimental study of Ref.[24] rely on a polycrystalline thin film, prepared by evaporation of Al-Co multi-layers followed by an appropriate annealing

treatment, the nominal Al:Co atomic ratio of the sample corresponding to 13:4 on average. Such surface probably presents an increased roughness as well as both structural and chemical heterogeneity compared to the homogeneous single crystal (100) surface considered in the calculations. In addition, the theoretical contact angle determined on (100) surface is on the same order of magnitude as the experimental angle measured for the $Pb/Al_{13}Co_4(010)$ system,[58] which reinforces the reliability of our prediction, the anisotropy of the contact angles being assumed to be small (see *Discussion* section).

3.2 Interfacial Energies and Electronic Structures

The theoretical interfacial energies are gathered in Tab. 2. For Pb(111)/Al(111), they are almost the same for all considered Pb-adlayer thicknesses, in agreement with the layer-by-layer growth of thick Al films described in Ref.[54] The situation is different in the case of the Al-Co quasicrystalline approximants. Here, the interfacial energy sharply increases from one to two Pb adlayers, and remains almost the same for three and four Pb adlayers. It shows an energetic cost for the growth of Pb thick films on such substrates. For $Pb/Al_{13}Co_4(100)$, this is in agreement with the experimental finding that Pb thin films do not grow in a layer-by-layer fashion on that surface.[56]

Interfacial Pb electronic structures are shown in Fig. 5 and Fig. S5 for different systems. They are compared to the ones of bulk Pb and of a freestanding Pb(111) single layer. The s and p bands of Pb bulk DOS extend over the [-11.5 eV ; -6.75 eV] region and from -4 eV. Such separation of the s and p states, observed in the bulk DOS, also occurs in the freestanding Pb single layer, since it is not structure induced.[52,59] This feature does not appear anymore for Pb deposited on the different substrates, probing the interaction of Pb states with the substrate Al states. For Al-Co compounds, a larger interaction is noticeable around -2 eV, due to hybridization with the Co d-states. The contribution of Pb atoms to the DOS of $Pb(111)/Al_5Co_2(001)$ exhibits a clear and faint minimum at the Fermi energy (called the

Table 2: Surface energies ($\gamma^{\text{substrate}}$, meV/Å^2), modified surface energies ($\gamma^{\text{substrate}}_{modified}$, meV/Å^2) and work functions ($W^{\text{substrate}}$, eV) for clean surfaces, as well as interfacial energies ($\gamma_n^{\text{interface}}$, meV/Å^2) as a function of the Pb-adlayer thickness ($n \in \{1,2,3,4\}$), for the Al(111), $Al_5Co_2(001)$, $Al_5Co_2(2\bar{1}0)$ and $Al_{13}Co_4(100)$ substrates (hexagonal-like models). [a] is the value obtained for the Pb(111)/Al(111) interface using a slab which does not contain any vacuum layer.

	Al(111)	$Al_{13}Co_4(100)$	$Al_5Co_2(001)$	$Al_5Co_2(2\bar{1}0)$
$\gamma^{\text{substrate}}$	50.1	65.6	83.8	87.6
$\gamma^{\text{substrate}}_{modified}$	37.6	40.9	55.2	55.4
$W^{\text{substrate}}$	3.85	4.26	4.02	4.37
$\gamma_1^{\text{interface}}$	19.7	23.1	37.4	37.7
$\gamma_2^{\text{interface}}$	22.1	37.6	55.6	54.7
$\gamma_3^{\text{interface}}$	23.4	32.2	57.7	58.6
$\gamma_4^{\text{interface}}$	23.0 (18.5[a])	42.3	58.3	56.7

pseudogap, Fig. 5). The pseudogap is present for the clean $Al_5Co_2(2\bar{1}0)$ and $Al_{13}Co_4(100)$ surfaces, but not visible when hexagonal- or pseudomorphic-like Pb-adlayer are present (Fig. 5).

4 Discussion

In this work, we determined interfacial energies for Pb/Al and Pb/Al-Co compounds, as a function of the Pb film thickness in the range from 1 to 4 layers. For Pb(111)/Al(111), our result (23.0 meV/Å^2) is in better agreement with the experimental value (13.5 meV/Å^2)[28] than the one of a previous theoretical study (28.3 meV/Å^2).[29] The interfacial structure considered in Ref.[29] was a Moiré structure as well, but different from the one determined experimentally. In addition, the modeling was based on empirical potentials, and did not consider any vacuum layer, avoiding the consideration of the lead surface energy. Using the same approach, but with the experimental Moiré structure, and DFT-based calculations, we obtained an interfacial energy equal to 18.5 meV/Å^2. The accuracies achieved on interfacial energies, leading to the determination of contact angles in good agreement with the experimental measurements, are due to the consideration of electronic effects on wetting. For

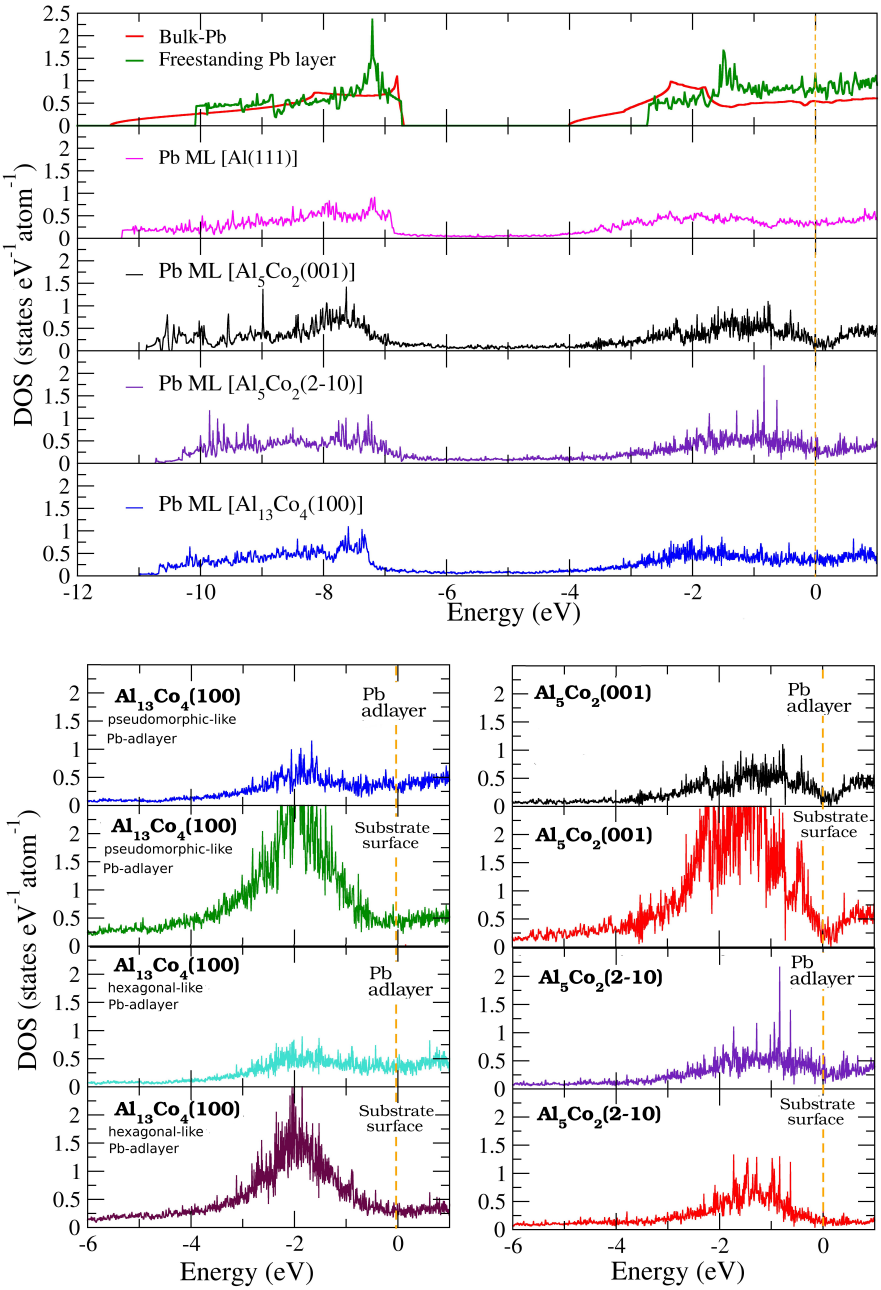

Figure 5: Top: Lead contribution to the density of states for one lead monolayer deposited on Al(111), $Al_5Co_2(001)$, $Al_5Co_2(2\bar{1}0)$, $Al_{13}Co_4(100)$. The DOS of a freestanding Pb layer is given for comparison, as well as the DOS of bulk Pb. Bottom : Contributions to the DOS from the surface layers of the $Al_{13}Co_4(100)$ and $Al_5Co_2(001)$ substrates, as well as from the first Pb adlayer. The interfacial structure is based on the hexagonal-like Pb-adlayer structure for $Al_{13}Co_4(100)$, $Al_5Co_2(2\bar{1}0)$ and $Al_5Co_2(001)$. For $Al_{13}Co_4(100)$, we also considered the pseudomorphic-like structure.

Pb(111)/Al(111) with the model of hexagonal layers, we determine a contact angle equal to 35^o, in good agreement with the experimental value (28 ± 7^o), while molecular dynamics calculations based on empirical potentials led to a higher value (46.4^o).[30] Besides electronic effects, the consideration of surface energies in our model is essential. Methods based on adsorption energies only,[48,60,61] althought they appear well adapted for the determination of water-wetting properties, are not adequate for the determination of wetting properties using a metal as a probe.

The previous example shows that the interface is crucial to determine the wetting properties. The consideration of a realistic structure for the first lead atomic layer on the substrate is important. Contact angles may be overestimated if the lowest energy configuration for the interface is not reached. In this work, we considered dense Pb-adlayers, with an interface built either on the basis of experimental observations (Pb(111)/Al(111)), or driven by the minimization of the lattice mismatch between the substrate and Pb(111). A rough estimation of the influence of the interface on contact angles was carried out for Pb/$Al_{13}Co_4$(100). Several interfacial structures were considered: hexagonal-like, pseudomorphic-like and MD-like. While results of the same order of magnitude were found for contact angles (94^o, 82^o and 116^o, respectively, Tab. S3 and S4), the lowest contact angle was determined in the case of the pseudomorphic-like structure, i.e. the more realistic one (a pseudomorphic growth was observed experimentally[56]). Our results using the hexagonal-like structure are not so different – they can be considered as acceptable. It is attributed to the balance arising from the adlayer-substrate interaction strength and from the adlayer atomic density (16 and 15 atoms per surface cell for the hexagonal-like and pseudomorphic-like structures, respectively).

The previous observations suggest that the aperiodic or periodic nature of the interface may influence the wetting features of decagonal quasicrystals. Using these materials, several properties have already been shown to be influenced by the periodic vs. aperiodic order, like optical conductivity[62] or friction.[63] In this work, contact angles and interfacial energies were found to be comparable for the pseudo-10fold $Al_5Co_2(2\bar{1}0)$ and the $Al_5Co_2(001)$ surfaces

(Tabs. 1-2). Here, we only considered an hexagonal-like interfacial structure for both orientations. While the interfacial structure adopted for $Al_5Co_2(001)$ may be the lowest energy configuration (a pseudogap is visible in the density of states, suggesting a pseudomorphic-like structure), no pseudogap is noticeable for $Al_5Co_2(2\bar{1}0)$, suggesting that a more realistic interface may lead to a smaller contact angle. It is indeed fulfilled by considering the P_{B-4Co} model for $Al_5Co_2(2\bar{1}0)$ (Tab. S5). However, from the knowledge gained by the analysis of $Pb/Al_{13}Co_4(100)$, no drastic difference ($\Delta\theta > 35^o$) is anticipated. We may then predict that the wetting anisotropy is rather small using quasicrystalline approximants, similarly to what was observed for simple metal/metal interfaces.[64]

Here, electronic interactions at the interface play a significant role. When dealing with two metals, like Pb(111)/Al(111), the bonding at the interface is metallic, as illustrated by the DOS calculations (Fig. 5). A slight charge transfer occurs (Tab. S6), not influenced by the thickness of the Pb-adlayer, and resulting from the small electronegativity difference between Al and Pb (1.61 and 1.87, respectively[65]). It leads to a rather high interaction energy ($E^{\text{interaction}}_{Pb/Al(111)}$=65.7 meV/Å^2), defined as $E^{\text{interaction}}_{Pb/substrate} = -E^{tot}_{Pb/substrate} + E^{tot}_{substrate} + E^{tot}_{Pb}$ where $E^{tot}_{Pb/substrate}$, $E^{tot}_{substrate}$ and E^{tot}_{Pb} are the total energies of the substrate covered with a lead single layer, the clean substrate and a free-standing Pb-adlayer. The good wetting observed for this system can then be attributed to this strong interaction.

When dealing with Pb deposited on the complex Al-Co intermetallic surfaces, the effect of the interface extends further into the intermetallic compound. Indeed, the Co d-states on the sub-interface now participate in the charge distribution (Tab. S6), as well as in orbital hybridization with the Pb sp-states (Fig. 5). The interaction between the Pb-adlayer and the substrate remains metallic, but with a non negligible iono-covalent character. Interfacial Al atoms behave as donor atoms (Fig. 6): the Bader charges carried by surface Al atoms increase from $0.23e$ and $0.67e$ for the clean $Al_{13}Co_4(100)$ and $Al_5Co_2(001)$ surfaces, respectively, to $0.36e$ and $0.76e$ for the surfaces covered with Pb, on average (Tab. S6, Fig. 6). This leads to a charge transfer towards interfacial Pb ($\Delta Q_{\text{Pb}} = -0.06e$) and subsurface Co atoms. The

Bader charges carried by subsurface Co atoms decrease from -3.26e and -2.92e for the clean $Al_{13}Co_4(100)$ and $Al_5Co_2(001)$ surfaces, respectively, to -3.42e and -3.05e for the surfaces covered with Pb, on average. The resulting interaction energy is rather large : $E^{\text{interaction}}_{Pb/Al_{13}Co_4(100)}$ = 80.5 meV/Å^2 and $E^{\text{interaction}}_{Pb/Al_5Co_2(001)}$ = 93.2 meV/Å^2. Such strong interactions however lead to a poor wetting behavior, demonstrating that the consideration of the interaction energy alone cannot explain our results.

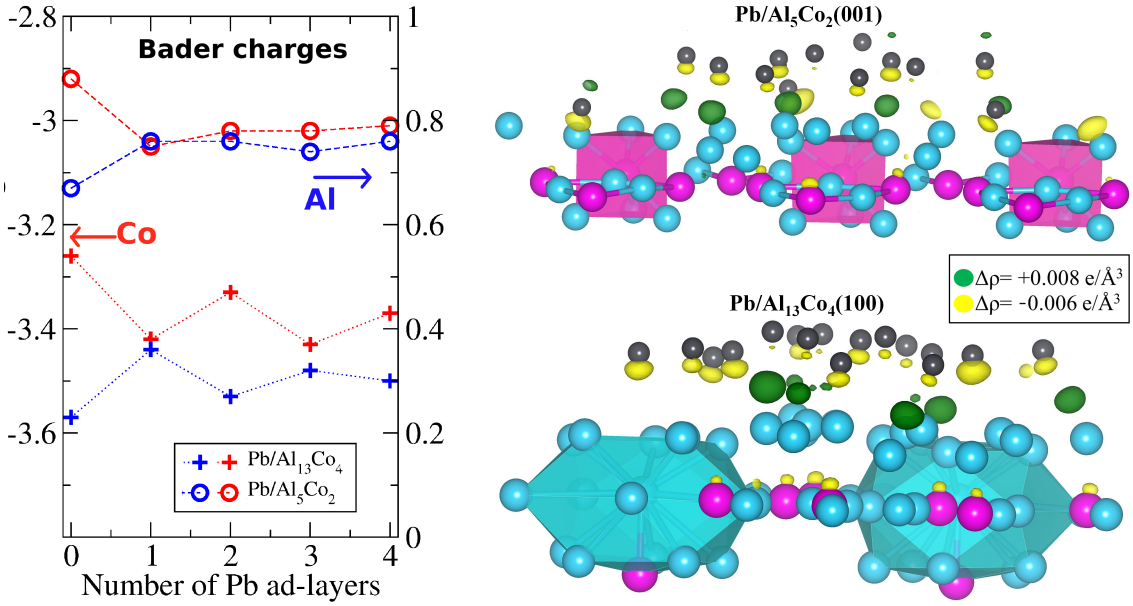

Figure 6: Bader charges for interfacial Al and Co atoms, as a function of the number of Pb-adlayers. Charge density deformation at the $Pb/Al_{13}Co_4(100)$ and $Pb/Al_5Co_2(001)$ interfaces.

Wetting is a tricky observable, depending on the interfacial energy between the substrate and the liquid, as well as on the surface energies of the substrate and the liquid. The factor $\Delta\gamma = \gamma^{substrate}_{modified} - \gamma_{interface}$ calculated to be positive for good wetting systems (+15 meV/Å^2 for Al(111)) and slightly negative for the Al-Co complex intermetallics (-1 meV/Å^2 for $Al_{13}Co_4(100)$, -3 meV/Å^2 for $Al_5Co_2(001)$ and -1 meV for $Al_5Co_2(2\bar{1}0)$). However, the calculation of such factor is not straightforward.

Electronic density of states at the Fermi energy ($n(E_F)$) is a key factor in condensed matter physics and material science that determines the properties of metals. It has already

been shown to drive the wetting properties of Cu deposited on different oxides.[66] The partial electronic density of states within the bulk material (n_{Al}^{3p}) has also been invoked to analyze the unique reversible adhesion energy of water on several Al-based intermetallics.[21] Surface energies are derived from $n(E_F)$,[67–70] within the free electron model, while interfacial energies depends on the work function differences ΔW between the two metals. The latter is small for low electron density metals ($\Delta W_{\mathrm{Al(111)/Pb(111)}} < 0.1$ eV, since $W_{\mathrm{Al(111)}}$=3.85 eV (our work) and $W_{\mathrm{Pb(111)}}$=3.78 eV[71]), the electronic transfer being facile between two metals. It is larger when considering the interface between lead and complex intermetallic compounds with small $n(E_F)$ ($W_{\mathrm{Al_5Co_2(001)}}$=4.02 eV, $W_{\mathrm{Al_{13}Co_4(100)}}$=4.26 eV), leading to larger interfacial energies.[70] One then expect $\Delta\gamma > 0$ for small ΔW and $\Delta\gamma < 0$ for larger ΔW. Considering lead as a probe, good wetting is then expected for good metals, i.e. presenting large $n(E_F)$, while poor wetting is predicted for compounds with small $n(E_F)$. It is in agreement with our observations: a small density of states at the Fermi energy corresponds to a larger value of the contact angle (Fig. 7).

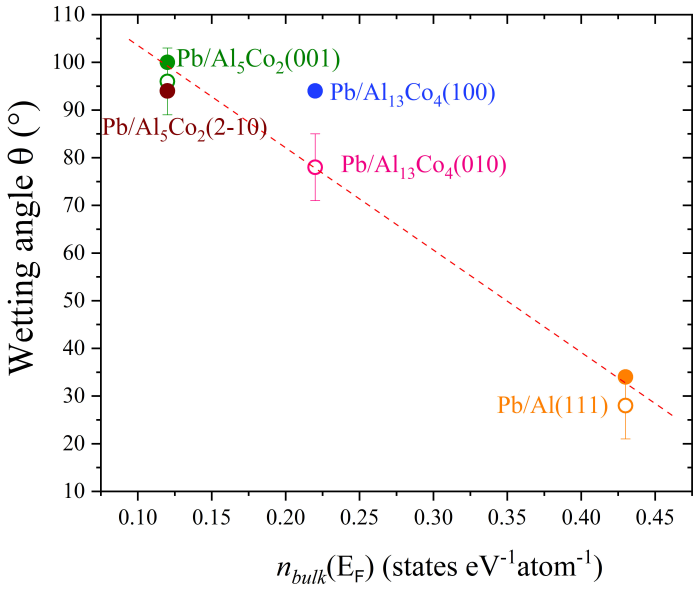

Figure 7: Contact angles plotted as a function of $n(E_F)$.

5 Conclusion

We reported the unexpected non-wetting behavior of liquid Pb metal droplets on two quasicrystalline approximants to decagonal quasicrystals, namely Al_5Co_2 and $Al_{13}Co_4$. Thanks to our theoretical model based on the Young equation, the intrinsic wettability of Al-Co compounds is predicted from first-principles, and validated by the good agreement with experimental measurements performed under ultra-high vacuum by scanning electron microscopy.

The wetting properties have been discussed in terms of geometric and electronic effects. For Pb(111)/Al(111), the high-order commensurate $(\sqrt{31} \times \sqrt{31})R8.95^o$ interface, as well as the common pure metallic character of the two elements, leads to a good wetting. The situation is different for Pb(111)/Al_5Co_2(001), Pb(111)/$Al_5Co_2(2\bar{1}0)$ and Pb(111)/$Al_{13}Co_4$(100), even if the Al-Co compound surfaces present an Al-rich termination. In these systems, the contact angles are large ($\sim 90^o$). The intrinsic non-wettability can be directly assigned to electronic effects and correlated through the density of states at the Fermi energy.

In summary, we have developed an approach to predict the intrinsic surface Pb-wettability of aluminum and two intermetallic compounds, based on a simple DFT slab model. As compared with MD simulations based on empirical potentials, the proposed first-principles method is much more efficient, since fewer input parameters are required and a rather good accuracy, at least a better agreement with experimental observations, is obtained. Although we consider pure Al and Al-Co quasicrystalline approximants as a benchmark in this study, the proposed method is very general and may be applicable to any crystal surfaces and non-reactive metal liquids. This paves the way for a better fundamental understanding of wettability, useful in a wide range of fields, like catalysis for metal-support interactions.

Conflicts of Interest

There are no conflicts to declare.

Supporting Information Available

Supporting information: Bulk and surfaces (thermodynamic results), Pb(111)/Al(111) (DOS and STM images), Bader charges

Acknowledgement

The authors thank Dr. M. Badawi for fruitful discussions about molecular dynamics calculations. We are very grateful to M.-C. de Weerd and our collaborators at the Ludwig Maximilians Universitt (P. Gilles group) who provided several single crystals. We aknowledge support from the European Consortium ECMetAC and funding from the COMETE project (COnception in silico de Matériaux pour l'EnvironnemenT et l'Energie) co-funded by the European Union under the program 'FEDER-FSE Lorraine et Massif des Vosges 2014-2020'. This work was granted access to the High Performance Computing (HPC) resources of TGCC, CINES, IDRIS under the allocation 99642 attributed by GENCI (Grand Equipement National de Calcul Intensif). HPC resources were partially provided by the EXPLOR center hosted by Université de Lorraine (grant M4XXX0108).

References

(1) Rosen, K.; Potash, M. Forty Years of Helicopter Ice Protection Experience At Sikorsky Aircraft. *J. Am. Helicopter Soc.* **1981**, *26*, 5–19.

(2) Ruan, M.; Li, W.; Wang, B.; Deng, B.; Ma, F.; Yu, Z. Preparation and Anti-icing Behavior of Superhydrophobic Surfaces on Aluminum Alloy Substrates. *Langmuir* **2013**, *29*, 8482–8491.

(3) Zuo, Z.; Liao, R.; Guo, C.; Yuan, Y.; Zhao, X.; Zhuang, A.; Zhang, Y. Fabrication and Anti-Icing Property of Coral-Like Superhydrophobic Aluminum Surface. *Appl. Surf. Sci.* **2015**, *331*, 132–139.

(4) Zhang, J.; Gu, C.; Tu, J. Robust Slippery Coating with Superior Corrosion Resistance and Anti-Icing Performance for AZ31B Mg Alloy Protection. *ACS Applied Materials & Interfaces* **2017**, *9*, 11247–11257.

(5) Qing, Y.; Hu, C.; Yang, C.; An, K.; Tang, F.; Tan, J.; Liu, C. Rough Structure of Electrodeposition as a Template for an Ultrarobust Self-Cleaning Surface. *ACS Applied Materials & Interfaces* **2017**, *9*, 16571–16580.

(6) Rahman, O.; Biswajyoti, M.; Aminul, I.; Keshri, A. Instant Tuning of Superhydrophilic to Robust Superhydrophobic and Self-Cleaning Metallic Coating: Simple, Direct, One-Step, and Scalable Technique. *ACS Appl. Mater. Interfaces* **2013**, *5*, 8495–8504.

(7) Feil, A. F.; Weibel, D. E.; Corsetti, R. R.; Pierozan, M. D.; Michels, A. F.; Horowitz, F.; Amaral, L.; ; Teixeira, S. R. Micro and Nano-Texturization of Intermetallic Oxide Alloys by a Single Anodization Step: Preparation of Artificial Self-Cleaning Surfaces. *ACS Applied Materials & Interfaces* **2011**, *3*, 3981–3987.

(8) Wang, X.-Z.; Luo, H.; Muneshwar, T.; Fan, H.-Q.; Cadien, K.; Luo, J.-L. Zr_2N_2O

Coating-Improved Corrosion Resistance for the Anodic Dissolution Induced by Cathodic Transient Potential. *ACS Applied Materials & Interfaces* **2018**, *10*, 40111–40124.

(9) Xie, Z.-H.; Li, D.; Skeete, Z.; Sharma, A.; Zhong, C.-J. Nanocontainer-Enhanced Self-Healing for Corrosion-Resistant Ni Coating on Mg Alloy. *ACS Applied Materials & Interfaces* **2017**, *9*, 36247–36260.

(10) Bi, C.; Wang, Q.; Shao, Y.; Yuan, Y.; Xiao, Z.; Huang, J. Non-Wetting Surface-Driven High-Aspect-Ratio Crystalline Grain Growth for Efficient Hybrid Perovskite Solar Cells. *Nature Communications* **2015**, *6*, 7747 (1to7).

(11) Matteini, F.; Ttncoglu, G.; Potts, H.; Jabeen, F.; i Morral, A. F. Wetting of Ga on SiO_x and Its Impact on GaAs Nanowire Growth. *Crystal Growth and Design* **2015**, *15*, 3105–3109.

(12) Ray, N.; Froyen, L.; Vanmeensel, K.; Vleugels, J. Wetting and Solidification of Silver Alloys in the Presence of Tungsten Carbide. *Acta Mater.* **2018**, *144*, 459–469.

(13) Nautiyal, P.; Gupta, A.; Seal, S.; Boesl, B.; Agarwal, A. Reactive Wetting and Filling of Boron Nitride Nanotubes By Molten Aluminum During Equilibrium Solidification. *Acta Mater.* **2017**, *126*, 124–131.

(14) Li, L.; Cao, K.-Z.; Shen, P.; Jiang, Q.-C. Roles of Direct Current in Ultrafast Wetting of 3YSZ By $Sn_{3.0}Ag_{0.5}Cu$ and Joining To Ni. *Materialia* **2019**, *7*, 100399.

(15) Wang, S.; Liu, K.; Yao, X.; Jiang, L. Bioinspired Surfaces with Superwettability: New Insight on Theory, Design, and Applications. *Chemical Reviews* **2015**, *115*, 8230–8293.

(16) Su, B.; Tian, Y.; ; Jiang, L. Bioinspired Interfaces with Superwettability: From Materials to Chemistry. *J. Am. Chem. Soc.* **2016**, *138*, 1727–1748.

(17) Anastasiadis, S. H. Development of Functional Polymer Surfaces with Controlled Wettability. *Langmuir* **2013**, *29*, 9277–9290.

(18) Schlaich, C.; Wei, Q.; Haag, R. Mussel-Inspired Polyglycerol Coatings with Controlled Wettability: From Superhydrophilic to Superhydrophobic Surface Coatings. *Langmuir* **2017**, *33*, 9508–9520.

(19) Eustathopoulos, N. Wetting by Liquid Metals-Application in Materials Processing: the Contribution of the Grenoble Group. *Metals* **2015**, *5*, 350–370.

(20) Cui, Y.; Liang, F.; Yang, Z.; Xu, S.; Zhao, X.; Ding, Y.; Lin, Z.; Liu, J. Metallic Bond-Enabled Wetting Behavior at the Liquid Ga/$CuGa_2$ Interfaces. *ACS Applied Materials & Interfaces* **2018**, *10*, 9203–9210.

(21) Dubois, J.-M. A Model of Wetting On Quasicrystals in Ambient Air. *Journal of Non-Crystalline Solids* **2004**, *334-335*, 481–485.

(22) Dubois, J. M. Properties and Applications of Quasicrystals and Complex Metallic Alloys. *Chem. Soc. Rev.* **2012**, *41*, 6760–6777.

(23) Bergman, C.; Girardeaux, C.; Perrin-Pellegrino, C.; Gas, P.; Dubois, J.-M.; Rivier, N. Contact Angles of Liquid Metals On Quasicrystals. *J. Phys.: Condens. Matter* **2008**, *20*, 314010 (1to7).

(24) Bergman, C.; Girardeaux, C.; Perrin-Pellegrino, C.; Gas, P.; Chatain, D.; Dubois, J.-M.; Rivier, N. Wetting of Decagonal $Al_{13}Co_4$ and Cubic AlCo Thin Films by Liquid Pb. *Philos. Mag.* **2006**, *86*, 849–854.

(25) Werder, T.; Walther, J.; Jaffe, R.; Halicioglu, T.; Noca, F.; Koumoutsakos, P. Molecular Dynamics Simulation of Contact Angles of Water Droplets in Carbon Nanotubes. *Nano Letters* **2001**, *1*, 697–702.

(26) Weijs, J. H.; Snoeijer, J. H.; Lohse, D. Formation of Surface Nanobubbles and the Universality of Their Contact Angles: A Molecular Dynamics Approach. *Phys. Rev. Lett.* **2012**, *108*, 104501.

(27) Reguera, J.; Ponomarev, E.; Geue, T.; Stellacci, F.; Bresme, F.; Moglianetti, M. Contact Angle and Adsorption Energies of Nanoparticles At the AirLiquid Interface Determined By Neutron Reflectivity and Molecular Dynamics. *Nanoscale* **2015**, *7*, 5665–5673.

(28) Shi, Z.; Lowekamp, J. B.; Wynblatt, P. Energy of the Pb(111)||Al(111) Interface. *Metallurgical and materials transactions* **2002**, *33A*, 1003–1007.

(29) Landa, A.; Wynblatt, P.; Johnson, E.; Dahmen, U. Computer Simulation of Pb/Al Interfaces. *Acta mater.* **2000**, *48*, 2557–2563.

(30) Zhao, Z.-Y.; Li, T.; Duan, Y.-R.; Wang, Z.-C.; Li, H. Wetting and Coalescence of the Liquid Metal On the Metal Substrate. *Chinese Phys. B 26*, 083104 (1to7).

(31) Meier, M.; Ledieu, J.; Weerd, M.-C. D.; Huang, Y.-T.; Abreu, G. J. P.; Diehl, R.; Mazet, T.; Vincent.Fournée,; Gaudry, E. Interplay Between Bulk Atomic Clusters and Surface Structure in Complex Intermetallic Compounds: the Case Study of the Al_5Co_2(001) Surface. *Phys. Rev. B* **2015**, *91*, 085414 (1to16).

(32) Gille, P.; Bauer, B. Single Crystal Growth of $Al_{13}Co_4$ and $Al_{13}Fe_4$ from Al-rich Solutions by the Czochralski Method. *Cryst. Res. Technol.* **2008**, *43*, 1161–1167.

(33) Shin, H.; Pussi, K.; Gaudry, É.; Ledieu, J.; Fournée, V.; Alarcón-Villaseca, S.; Dubois, J.-M.; Grin, Y.; Gille, P.; Moritz, W.; Diehl, R. Structure of the Orthorhombic $Al_{13}Co_4$(100) Surface Using LEED, STM and Ab Initio Studies. *Phys. Rev. B* **2011**, *84*, 085411 (1to11).

(34) Blochl, P. E. Projector Augmented-Wave Method. *Phys. Rev. B* **1994**, *50*, 17953–17979.

(35) Kresse, G.; Joubert, D. From Ultrasoft Pseudopotentials To the Projector Augmented-Wave Method. *Phys. Rev. B* **1999**, *59*, 1758–1775.

(36) Monkhorst, H. J.; Pack, J. D. Special Points for Brillouin-Zone Integrations. *Phys. Rev. B* **1976**, *13*, 5188–5192.

(37) Perdew, J. P.; Burke, K.; Ernzerhof, M. Generalized Gradient Approximation Made Simple. *Phys. Rev. Lett.* **1996**, *77*, 3865.

(38) Perdew, J. P.; Burke, K.; Ernzerhof, M. Erratum: Generalized Gradient Approximation Made Simple. *Phys. Rev. Lett.* **1997**, *78*, 1396.

(39) Scheid, P.; Chatelier, C.; Ledieu, J.; Fournée, V.; Gaudry, E. Bonding Network and Stability of Clusters: The Case Study of the $Al_{13}TM_4$ Pseudo-10fold Surfaces. *Acta Crystallogr. A* **2019**, *75*, 314–324.

(40) Meier, M.; Ledieu, J.; Fournée, V.; Gaudry, E. Semi-Hydrogenation of Acetylene On Al_5Co_2 Surfaces. *J. Phys. Chem. C* **2017**, *121*, 4958–4969.

(41) Kandaskalov, D.; Fournée, V.; Ledieu, J.; Gaudry, E. Catalytic Semihydrogenation of Acetylene on the (100) Surface of the o-$Al_{13}Co_4$ Quasicrystalline Approximant: Density Functional Theory Study. *J. Phys. Chem. C* **2017**, *121*, 18738–18745.

(42) Burkhardt, U.; Ellner, M.; Grin, Y.; Baumgartner, B. Powder Diffraction Refinement of the Co_2Al_5 Structure. *Powder Diffr.* **1998**, *13*, 159–162.

(43) Grin, J.; Burkhardt, U.; Ellner, M.; Peters, K. Crystal Structure of Orthorhombic Co_4Al_{13}. *J. Alloys Compd.* **1994**, *206*, 243–247.

(44) Meier, M.; Ledieu, J.; Weerd, M.-C. D.; Fournée, V.; Gaudry, E. Structural Investigations of $Al_5Co_2(2\bar{1}0)$ and (100) Surfaces: Influence of Bonding Strength and Annealing Temperature On Surface Terminations. *Phys. Rev. B* **2016**, *93*, 075412 (1to11).

(45) Gaudry, E.; Chatelier, C.; McGuirk, G.; Loli, L. S.; DeWeerd, M.-C.; Ledieu, J.; Fournée, V.; Felici, R.; Drnec, J.; Beutier, G.; de Boissieu, M. Structure of the

$Al_{13}Co_4$(100) Surface: Combination of Surface X-Ray Diffraction and Ab Initio Calculations. *Phys. Rev. B* **2016**, *94*, 165406.

(46) Ledieu, J.; Gaudry, E.; de Weerd, M.-C.; Diehl, R. D.; Fournée, V. The (100) Surface of the $Al_{13}Co_4$ Quasicrystalline Approximant. *Mater. Res. Soc. Symp. Proc.* **2012**, *1517*.

(47) Jiang, H.; Patel, A. Recent Advances in Estimating Contact Angles Using Molecular Simulations and Enhanced Sampling Methods. *Current Opinion in Chemical Engineering* **2019**, *23*, 130–137.

(48) Lu, J.; Ge, Q.; Li, H.; Raza, A.; Zhang, T. Direct Prediction of Calcite Surface Wettability with First-Principles Quantum Simulation. *The Journal of Physical Chemistry Letters* **2017**, *8*, 5309–5316.

(49) Dupré, A. *Théorie Mécanique de la Chaleur*; Gauthier-Villars: Paris, 1869.

(50) Young, T. An Essay on the Cohesion of Fluids. *Philosophical Transactions of the Royal Society of London* **1805**, *95*, 65–87.

(51) Schwaneke, A.; Falke, W. Surface Tension and Density of Liquid Lead. *Journal of Chemical and Engineering Data* **1972**, *17*, 291–293.

(52) Jank, W.; Hafner, J. Structural and Electronic Properties of the Liquid Polyvalent Elements: the Group-IV Elements Si, Ge, Sn, and Pb. *Physical Review B* **1990**, *41*, 1497–1515.

(53) Bombis, C.; Emundts, A.; Nowicki, M.; Bonzel, H. Absolute Surface Free Energies of Pb. *Surface Science* **2002**, *511*, 83–96.

(54) Deniozou, T.; Ledieu, J.; Fournée, V.; Wu, D.; Lograsso, T. A.; Li, H. T.; Diehl, R. D. Aperiodic and Modulated Pb Thin Films on Fivefold Icosahedral Al-Cu-Fe and Al(111): Tailoring the Structure of Pb. *Phys. Rev. B* **2009**, *79*, 245405 (1to9).

(55) Alarcón-Villaseca, S.; Dubois, J.-.-M.; Gaudry, E. Lead Adsorption On the Pseudo-Tenfold Surface of the $Al_{13}Co_4$ Complex Metallic Alloy: A First Principle Study. *Int. J. Quantum Chem.* **2013**, *113*, 840–846.

(56) Addou, R.; Shukla, A. K.; Alarcón-Villaseca, S.; Gaudry, É.; Deniozou, T.; Heggen, M.; Feuerbacher, M.; Widmer, R.; Gröning, O.; Fournée, V.; Dubois, J.-M.; Ledieu, J. Lead Adsorption on the $Al_{13}Co_4$ (100) Surface: Heterogeneous Nucleation and Pseudomorphic Growth. *New Journal of Physics* **2011**, *13*, 103011 (1to19).

(57) Villaseca, S. A.; Loli, L. S.; Ledieu, J.; Fournée, V.; Gille, P.; Dubois, J.-M.; Gaudry, E. Oxygen Adsorption on the Al_9Co_2(001) Surface: First-Principles and STM Study. *J. Phys.: Condens. Matter* **2013**, *25*, 355003 (1to8).

(58) Anand, K. Surface Properties of Complex Intermetallics at the Nanoscale : from Fundamentals to Applications. Ph.D. thesis, Univ. Lorraine, 2018.

(59) Krajčí, M.; Hafner, J.; Ledieu, J.; Fournée, V.; McGrath, R. Quasiperiodic Pb Monolayer on the Fivefold *i*-Al-Pd-Mn Surface: Structure and Electronic Properties. *Phys. Rev. B* **2010**, *82*, 085417 (1to11).

(60) Lange, B.; Posner, R.; Pohl, K.; Thierfelder, C.; Grundmeier, G.; Blankenburg, S.; Schmidt, W. Water Adsorption on Hydrogenated Si(111) Surfaces. *Surf. Sci.* **2009**, *603*, 60–64.

(61) Carchini, G.; García-Melchor, M.; Lodziana, Z.; López, N. Understanding and Tuning the Intrinsic Hydrophobicity of Rare-Earth Oxides: A DFT+U Study. *ACS Appl. Mater. Interfaces* **2016**, *8*, 152–160.

(62) Basov, D. N.; Timusk, T.; Barakat, F.; Greedan, J.; Grushko, B. Anisotropic Optical Conductivity of Decagonal Quasicrystals. *Phys. Rev. Lett.* **1994**, *72*, 1937.

(63) Park, J. Y.; Ogletree, D. F.; Salmeron, M.; Ribeiro, R. A.; Canfield, P. C.; Jenks, C. J.; Thiel, P. A. High Frictional Anisotropy of Periodic and Aperiodic Directions on a Quasicrystal Surface. *Science* **2005**, *309*, 1354.

(64) Chatain, D.; Metois, J. A New Procedure for the Determination of the Free Energies of Solid-Fluid Interfaces From the Anisotropy of Wetting of A Melt On Its Solid. *Surf. Sci.* **1993**, *291*, 1–13.

(65) Haynes, W. M., Ed. *CRC Handbook of Chemistry and Physics*; CRC Press/Taylor and Francis: Boca Raton, USA.

(66) Eustathopoulos, N.; Nicholas, M.; Drevet, B. *Wettability at High Temperatures*; Pergamon Press: Amsterdam-Lausanne-New-York-Oxford-Shannon-Singapore-Tokyo, 1999.

(67) Lang, N. D.; Kohn, W. Theory of Metal Surfaces: Charge Density and Surface Energy. *Phys. Rev. B* **1970**, *1*, 4555–4568.

(68) Lang, D.; Kohn, W. Theory of Metal Surfaces: Work Function. *Phys. Rev. B* **1971**, *3*, 1215–1223.

(69) Muscat, J.; Allan, G. Interface Energy of Two Free-Electron-Like Metals. *J. Phys. F: Met. Phys.* **1977**, *7*, 999–1008.

(70) Wu, B.; Zhang, Z. Stability of Metallic Thin Films Studied with a Free Electron Model. *Phys. Rev. B* **2008**, *77*, 035410 (1to12).

(71) Yu, D.; Scheffler, M. First-Principles Study of Low-Index Surfaces of Lead. *Phys. Rev. B* **2004**, *70*, 155417 (1to9).

Supporting Information

Non-Wetting Behavior of Al-Co Quasicrystalline Approximants Owing to their Unique Electronic Structures

Kanika Anand[1,2], Vincent Fournée[1], Geoffroy Prévot[3], Julian Ledieu[1], Émilie Gaudry[1*]

[1] *Université de Lorraine, CNRS, IJL, F-54000 Nancy, France*

[2] *CIRIMAT, Université de Toulouse, CNRS, INPT, UPS, 4 Allée Emile Monso, BP44362, 31030 Toulouse Cedex 4, France*

[3] *Sorbonne Université, CNRS, Institut des NanoSciences de Paris, 4 place Jussieu, 75005 Paris, France*

E-mail: emilie.gaudry@univ-lorraine.fr

*To whom correspondence should be addressed

List of Figures

List of Tables

Auger Spectra

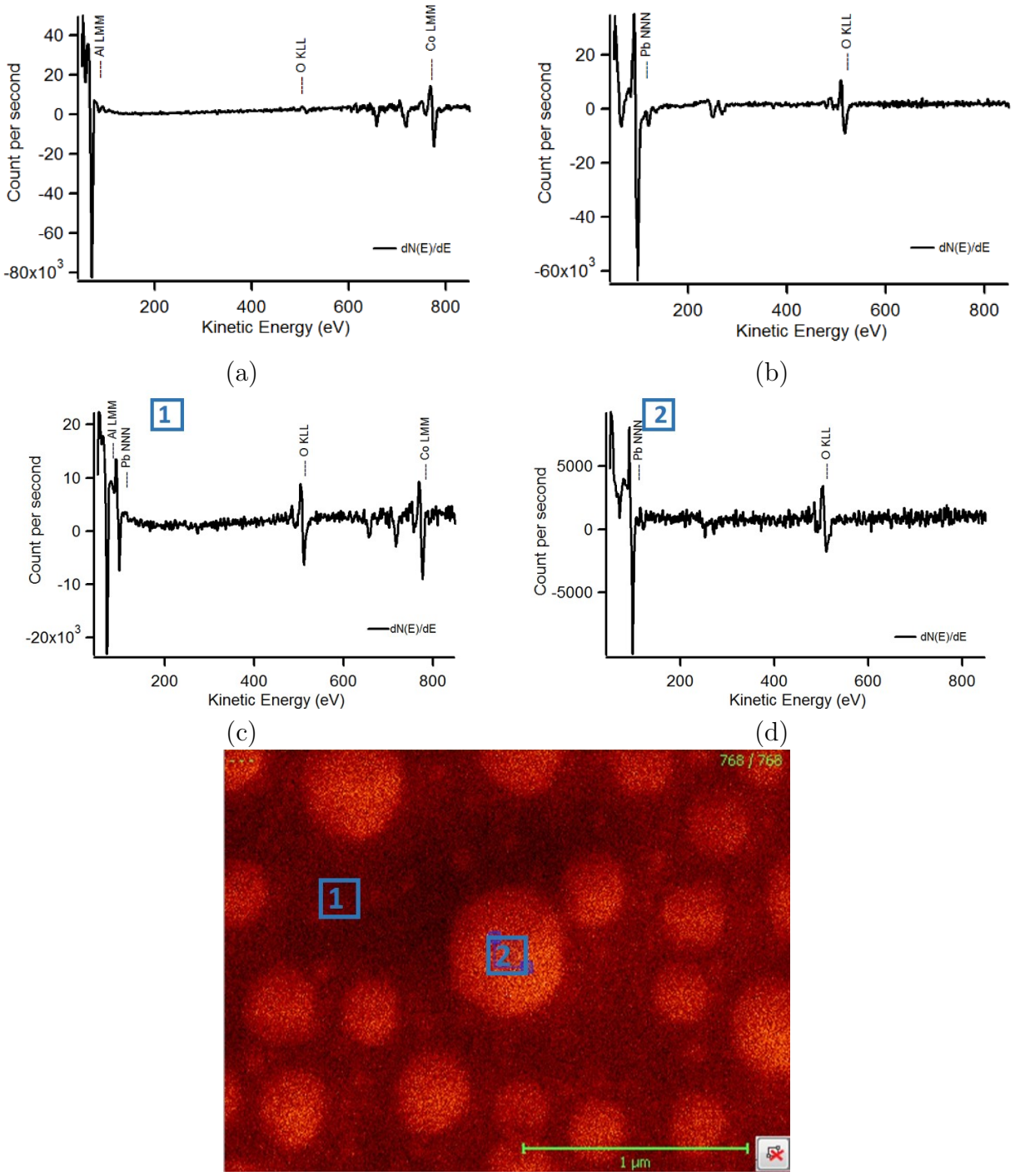

Figure S1: Top: Auger spectra of the clean $Al_5Co_2(001)$ surface (a), of the Pb film before dewetting (b) and after dewetting (c,d). Bottom: SEM image after dewetting.

Contact Angle Measurements

Contact angles were measured as schematically described in Fig. 2. We calculated the average contact angle (θ_{avg}, Fig. S2), i.e. the average of the apparent angle values (θ_{app}) and the fitted angle values (θ_{fit}, determined from curve-fitting) to avoid any errors due to local distortions or errors subjective to points chosen for curve fitting.[1] The average contact angle values were found to be independent of the droplet size as well as of the tilt angle.

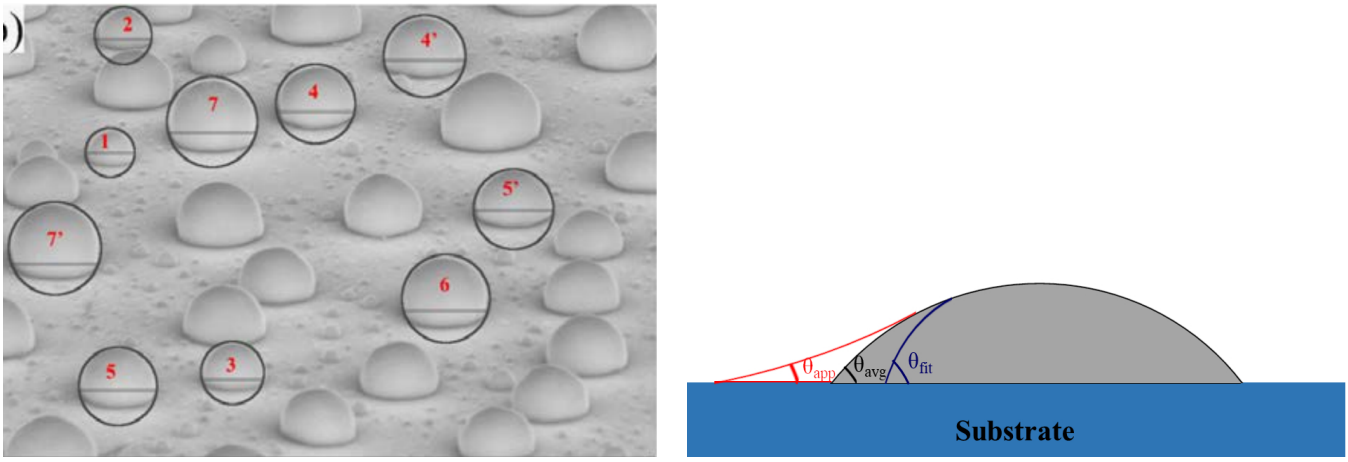

(a) (b)

Figure S2: (a) SEM micrograph showing Pb droplets on $Al_5Co_2(001)$. A few droplets are curve-fitted (black circles) for contact angle measurements. The red labels are used to identify the droplets of Tab. S1. (b) Schematic representation of the different contact angles mentioned in the text.

Table S1: Contact angle measurement for Pb/$Al_5Co_2(001)$.

	Droplet size (μm)	Contact angles (degrees)		
		θ_{fit}	θ_{app}	θ_{avg}
1	1.36	98.6	85.4	92
2	1.62	101.3	86.3	93.8
3	1.78	101.8	85.9	93.85
4	2.04	102.8	86.7	94.75
5	2.29	103.3	88.5	95.56
6	2.38	108.9	89.8	99.35
7	2.41	109.1	89.6	99.5

Surface Energy Calculations

According to Ref.,[2] the surface energy γ_{clean} of an elemental metal can be calculated using the following method. We consider a solid with a finite number n of infinitely extended planar atomic layers, and a slab of finite area A embedded in this solid. The slab has n layers, each with N_ℓ atoms. The surface energy is given by

$$\gamma_{clean} = \lim_{n\to\infty} \frac{E_{slab(n)} - nN_\ell E_{bulk}}{2A} \tag{1}$$

where $E_{slab}(n)$ is the total energy of the slab and E_{bulk} is the energy per atom of the infinite bulk. The factor of $\frac{1}{2}$ in this equation comes from the fact that the slab is bounded by two symmetric surfaces.

In the case of compounds, the stoichiometry of the slab is in general different from the one of the bulk. The surface energy is then determined as a function of the chemical potentials.[3] The chemical potential of species i (μ_i) is defined as the derivative of the Gibbs free enthalpy G for a given phase with respect to the number of particles i and fixed numbers of other particles $\{N_j\}$ apart from N_i:

$$\mu_i = \left(\frac{\partial G}{\partial N_i}\right)_{P,T,N_j} \tag{2}$$

For condensed states, the Gibbs free enthalpy per particle can be taken as the total energy per atom calculated at $T = 0$ K, i.e. as the cohesive energy (E_{coh} = the energy required to separate the elements into neutral atoms at $T = 0$ K and atmospheric pressure P). Indeed, the Gibbs free enthalpy $G(T, P, N)$ can be expressed using the Helmoltz free energy $F(T, V, N)$: $G(T, P, N) = F(T, V, N) + PV$. Under normal pressure ($\simeq$1 atm), the difference between the Helmholtz free energy F and the Gibbs free energy G ($F - G = -PV$) is almost zero for a solid. In addition, the temperature-dependent term is assumed to be negligible, based on the argument that there is a partial cancellation of the TS term (S is the entropy) with the contributions of the lattice vibrations to the internal energies ($3k_BT\sum N_i$) , at least in the limit of the validity of the equipartition theorem.

In the case of a simple metal, the previous statements imply that the chemical potential is simply given by the cohesive energy. For exemple, the chemical potential for Al in bulk Al is $\mu_{\mathrm{Al}}^{bulk} = E_{coh}^{\mathrm{Al}}$. In the case of a compound, the chemical potential is given by the Gibbs phase rule (equilibrium conditions). For $\mathrm{Al}_x\mathrm{Co}_y$, it implies that : $(x+y)\mu_{\mathrm{Al}_x\mathrm{Co}_y}^{bulk} = x\mu_{\mathrm{Al}} + y\mu_{\mathrm{Co}}$ where μ_{Al} and μ_{Co} are the chemical potentials of Al and Co in $\mathrm{Al}_x\mathrm{Co}_y$.

When compound surfaces are modeled with symmetric slabs, the surface energies are given by

$$\gamma_{clean} = \lim_{slab} \frac{E(N_i) - \sum N_i \mu_i}{2A} \tag{3}$$

where μ_i and N_i are the chemical potentials and number of atoms of type i in the slab. In the previous equation, the numerator can be understood as the difference between the total energy of the slab and the energy of the corresponding bulk with the same stoichiometry.

Bulk, Surfaces and Interfaces: Thermodynamic Results

Table S2: Cell parameters, cohesive energies and (111) surface energies of Al and Pb metals.

	a (Å)	E_{coh} (eV/at.)	$\gamma_{(111)}$ (meV/Å^2)	
Al	4.04	-3.50	50.1	calc.
Al	4.04[4]	-3.43[4]	55.5[2]	calc.
Al	4.04[5]	-3.39[6]	71.1[7]	exp.
Pb	5.03	-2.94	17.8	calc.
Pb	5.05[4]	-2.92[4]	17.2[8]	calc.
Pb	4.95[5]	-2.03[9]	27.5[10]	exp.

Table S3: Surface structures and energies (meV/Å^2, calculated with $\mu_{Al} = \mu_{Al}^{bulk}$) for pristine surfaces considered in this work. The labels are those used in previous references. According to Ref.,[13] two models (P_{B-4Co} and P_B) are conceivable for $Al_5Co_2(2\bar{1}0)$. The comparison between experimental and simulated STM images does not allow any discrimination between these two models, which differ by the number of protruding surface Co atoms. In this work, we built a surface model which locally presents at the surface the atomic arrangements of both P_{B-4Co} and P_B models.

Surface	$Al_{13}Co_4(100)$		$Al_5Co_2(001)$	$Al_5Co_2(2\bar{1}0)$	
Surface cell	(1×1)		$(\sqrt{3}\times\sqrt{3})$R30^o	(2×1)	
Model	$P_{24}^{\mathrm{Al,Co^-}}$ (Ref.[11])	P_{22}^{Al}(Ref.[11])	$P_{6\ \mathrm{Al\ miss}}^{\sqrt{3}\times\sqrt{3}R30^o}$ (Ref.[12])	P_{B-4Co} (Ref.[12])	$\langle P_{B-4Co}, P_B\rangle$
Our work	68.1	65.6	83.8	78.6	87.6
Refs.	68.0[11]		83.6[12]	79.3[12]	

Table S4: Interfacial and modified surface energies (meV/Å^2) for Pb/$Al_{13}Co_4(100)$ models considered in this work.

	hexagonal-like	pseudomorphic-like	MD-like
$\gamma_{modified}^{\mathrm{substrate}}$	40.9	40.6	36.7
$\gamma_1^{\mathrm{interface}}$	23.1	38.1	18.9
$\gamma_4^{\mathrm{interface}}$	42.3	38.0	44.5

Table S5: Interfacial energies (meV/Å^2) for Pb/$Al_5Co_2(2\bar{1}0)$ (P_{B-4Co} model).

Pb-adlayer thickness	$\gamma^{\text{interface}}$	θ
1	36.0	
2	52.7	86
3	51.3	82
4	47.1	68

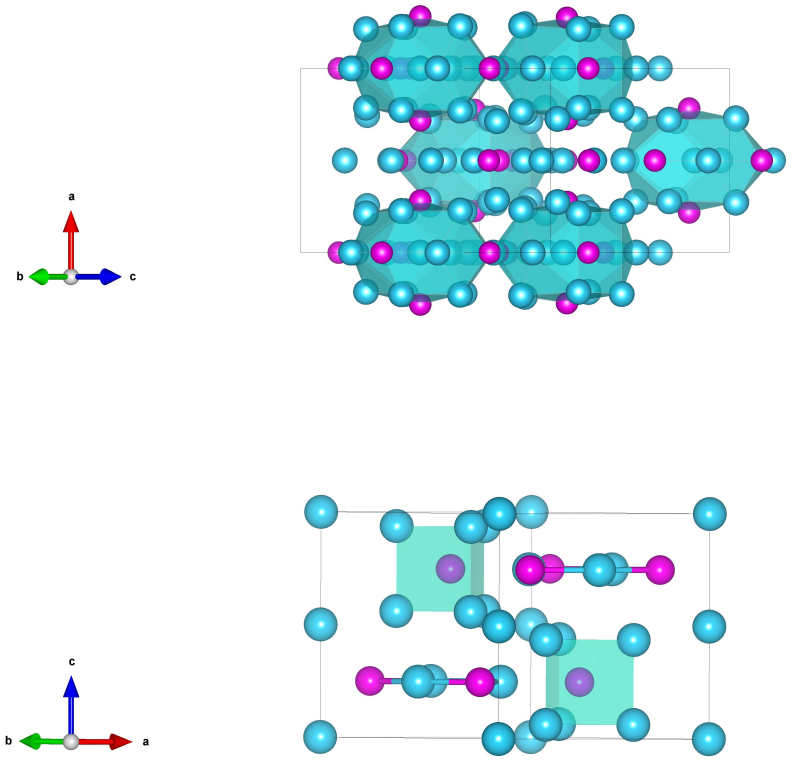

Figure S3: Bulk structures of $Al_{13}Co_4$ (top) and Al_5Co_2 (bottom). Color code: Al=blue; Co=magenta.

Pb(111)/Al(111) : DOS and STM Images

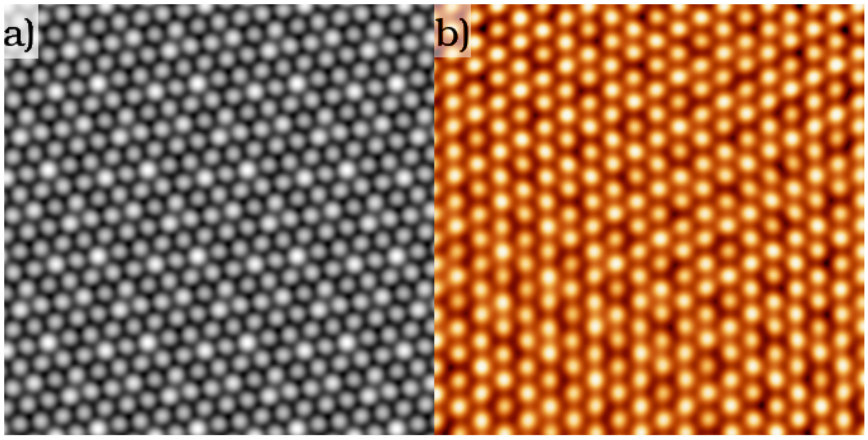

Figure S4: Theoretical (a) and Fourier filtered experimental (b) STM images ($V_{bias} = -0.5$ eV, 6×6 nm^2) for a lead monolayer over Al(111).

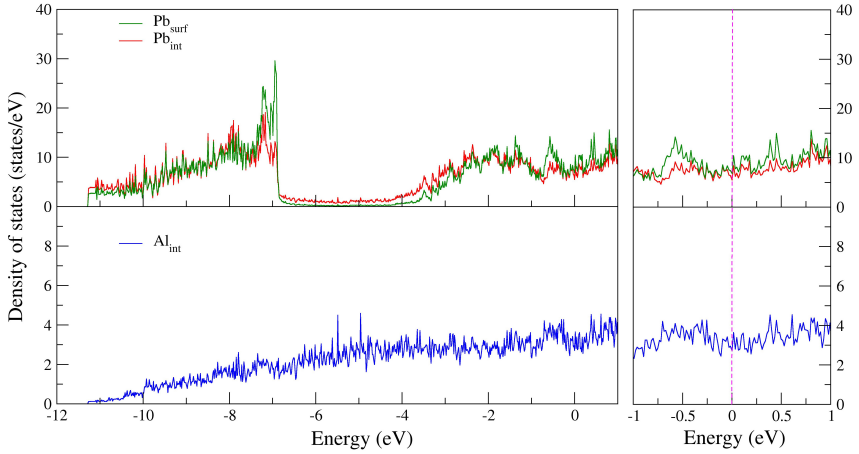

Figure S5: DOS for Pb(111)/Al(111). The considered system is built with 2 Pb-adlayers over the Al(111) substrate. The contributions of the Pb interfacial layer and the topmost Pb layer are shown in red and green, respectively. The contribution of the interfacial Al layer is shown in blue.

Bader Charges

Table S6: Bader charges ΔQ_x carried by interfacial atoms. The value is averaged over the atoms of the considered layer.

System	Nb	Pb_{int}	Al_{int}	$Al_{int\text{-}1}$	$Co_{int\text{-}1}$
Pb(111)/Al(111)	1	−0.04	0.02	0.02	-
Pb(111)/Al(111)	2	−0.04	0.02	0.00	-
Pb(111)/Al(111)	3	−0.04	0.02	0.01	-
Pb(111)/Al(111)	4	−0.05	0.02	0.01	-
$Al_{13}Co_4(100)$			0.23 ± 0.08	0.94 ± 0.10	-3.26 ± 0.20
Pb(111)/$Al_{13}Co_4$(100)	1	−0.06	0.36	1.00	−3.42
Pb(111)/$Al_{13}Co_4$(100)	2	−0.08	0.27	1.00	−3.33
Pb(111)/$Al_{13}Co_4$(100)	3	−0.06	0.32	1.00	−3.43
Pb(111)/$Al_{13}Co_4$(100)	4	−0.10	0.30	1.00	−3.37
$Al_5Co_2(001)$			0.67 ± 0.20	1.24 ± 0.05	-2.92 ± 0.45
Pb(111)/Al_5Co_2(001)	1	−0.06	0.76	1.25	−3.05
Pb(111)/Al_5Co_2(001)	2	−0.08	0.76	1.27	−3.02
Pb(111)/Al_5Co_2(001)	3	−0.06	0.74	1.26	−3.02
Pb(111)/Al_5Co_2(001)	4	−0.10	0.76	1.26	−3.01

References

(1) Kaplan, W.; Chatain, D.; Wynblatt, P.; Carter, W. C. A Review of Wetting Versus Adsorption, Complexions, and Related Phenomena: the Rosetta Stone of Wetting. *J. Mater. Sci.* **2013**, *48*, 5681–5717.

(2) Patra, A.; Bates, J. E.; Sun, J.; Perdew, J. P. Properties of Real Metallic Surfaces: Effects of Density Functional Semilocality and Van der Waals Nonlocality. *PNAS* **2017**, *114*, E91.

(3) Bechstedt, F. *Principles of Surface Physics*; Springer: Berlin, 2003.

(4) Lejaeghere, K.; Speybroeck, V. V.; Oost, G. V.; Cottenier, S. Error Estimates for Solid-State Density-Functional Theory Predictions: an Overview by Means of the Ground-State Elemental Crystals. *Critical Reviews in Solid State and Materials Sciences* **2014**, *39*, 1–24.

(5) Villars, P.; Cenzual, K. *Pearsons Crystal Data - Crystal Structure Database for Inorganic Compounds, Release 2012/13*; Materials Park, Ohio, USA: ASM International, 2013.

(6) Boer, F. D.; Boom, R.; Mattens, W.; Miedema, A.; Niessen, A. *Cohesion in Metals*; Elsevier, Amsterdam, 1988.

(7) Tyson, W.; Miller, W. Surface free energies of solid metals: Estimation from Liquid Surface Tension Measurements. *Surf. Sci.* **1977**, *62*, 267.

(8) Yu, D.; Scheffler, M. First-Principles Study of Low-Index Surfaces of Lead. *Phys. Rev. B* **2004**, *70*, 155417 (1to9).

(9) Kittel, C. *Introduction to Solid State Physics*, 7th ed.; John Wiley & Sons: USA, 1996.

(10) Bombis, C.; Emundts, A.; Nowicki, M.; Bonzel, H. Absolute Surface Free Energies of Pb. *Surface Science* **2002**, *511*, 83–96.

(11) Gaudry, E.; Chatelier, C.; McGuirk, G.; Loli, L. S.; DeWeerd, M.-C.; Ledieu, J.; Fournée, V.; Felici, R.; Drnec, J.; Beutier, G. et al. Structure of the $Al_{13}Co_4(100)$ Surface: Combination of Surface X-Ray Diffraction and Ab Initio Calculations. *Phys. Rev. B* **2016**, *94*, 165406.

(12) Meier, M.; Ledieu, J.; Fournée, V.; Gaudry, E. Semi-Hydrogenation of Acetylene On Al_5Co_2 Surfaces. *J. Phys. Chem. C* **2017**, *121*, 4958–4969.

(13) Meier, M.; Ledieu, J.; Weerd, M.-C. D.; Huang, Y.-T.; Abreu, G. J. P.; Diehl, R.; Mazet, T.; Vincent.Fournée,; Gaudry, E. Interplay Between Bulk Atomic Clusters and Surface Structure in Complex Intermetallic Compounds: the Case Study of the $Al_5Co_2(001)$ Surface. *Phys. Rev. B* **2015**, *91*, 085414 (1to16).